Club cells surviving influenza A virus infection induce temporary nonspecific antiviral immunity

Jennifer R. Hamilton[a], David Sachs[b], Jean K. Lim[a], Ryan A. Langlois[a,c], Peter Palese[a,d], and Nicholas S. Heaton[a,e,1]

[a]Department of Microbiology, Icahn School of Medicine at Mount Sinai, New York, NY 10029; [b]Department of Genetics and Genomic Sciences, Icahn School of Medicine at Mount Sinai, New York, NY 10029; [c]Department of Microbiology and Immunology, University of Minnesota Medical School, Minneapolis, MN 55455; [d]Department of Medicine, Icahn School of Medicine at Mount Sinai, New York, NY 10029; and [e]Department of Molecular Genetics and Microbiology, Duke University, Durham, NC 27710

Edited by Robert A Lamb, The Howard Hughes Medical Institute and Northwestern University, Evanston, IL, and approved February 23, 2016 (received for review November 12, 2015)

A brief window of antigen-nonspecific protection has been observed after influenza A virus (IAV) infection. Although this temporary immunity has been assumed to be the result of residual nonspecific inflammation, this period of induced immunity has not been fully studied. Because IAV has long been characterized as a cytopathic virus (based on its ability to rapidly lyse most cell types in culture), it has been a forgone conclusion that directly infected cells could not be contributing to this effect. Using a Cre recombinase-expressing IAV, we have previously shown that club cells can survive direct viral infection. We show here not only that these cells can eliminate all traces of the virus and survive but also that they acquire a heightened antiviral response phenotype after surviving. Moreover, we experimentally demonstrate temporary nonspecific viral immunity after IAV infection and show that surviving cells are required for this phenotype. This work characterizes a virally induced modulation of the innate immune response that may represent a new mechanism to prevent viral diseases.

influenza virus | RNA sequencing | alternative cell fate | antiviral immunity

There have been reports of a short period after influenza A virus (IAV) infection during which subsequent respiratory viral infection is restricted. This phenomenon has been shown experimentally in animal models (1–3), as well as in humans given the live-attenuated IAV vaccine in clinical studies (4–7), and has been postulated as a major factor in determining the rate of IAV antigenic drift (8). This temporary immunity has also been observed epidemically when the respiratory syncytial virus season was delayed as a result of the 2009 pandemic IAV outbreak occurring earlier than is normally seen with seasonal strains (9–11). Although observations of influenza-induced temporary immunity are well documented, how this protection is established is unknown.

We have previously shown that respiratory epithelial cells (principally club cells) are infected by IAV and are capable of clearing infection and surviving for long periods in vivo (12). These surviving cells, characterized by an inflammatory transcriptional profile, contributed to bronchiolar epithelium damage. However, it was unclear why these cells would prolong an inflammatory state beyond the resolution of infection.

In this report, we test the hypothesis that cells surviving IAV infection are involved in protecting the host from subsequent viral respiratory infections. We reasoned that the turnover of "survivor cells" could explain the temporary nature of IAV-induced antiviral immunity. We show that the cells that survive direct IAV infection are reprogrammed and exhibit an increased antiviral response to secondary infection and type I IFN. We also show that the overall immune response to secondary infection is different from the response to the primary infection. Finally, we demonstrate temporary, antigen-nonspecific viral immunity in the mouse model and show that surviving cells are required for this protection.

Results

To study the cells surviving IAV infection, we developed an in vitro reporter system. The human club cell-like line H441 was transduced with a lentiviral construct that induces production of ZsGreen protein after Cre recombinase activity (Fig. 1*A*). Shortly after infection with an H1N1 (A/Puerto Rico/8/1934) IAV expressing Cre (IAV-Cre) (12), infected cells produced both ZsGreen and viral protein (Fig. S1). Fourteen days postinfection, we detected a population of viable surviving cells (Fig. 1*B*). We sorted ZsGreen-positive cells over a time course and performed transcriptome analysis. These cells express high levels of viral mRNA immediately after infection, but virus is cleared by 2 wk postinfection (Fig. 1*C*). We also performed quantative (q)RT-PCR to detect viral RNA at 2 and 14 d postinfection and observed the same clearance kinetics (Fig. 1*D*).

We next investigated how cells were responding during viral replication and after viral clearance. Ordering the data by the most up-regulated genes (relative to preinfection) shows an early establishment of antiviral and stress response genes; resolution of this state occurs when viral RNA is eliminated (Fig. 1*E*). Interestingly, after the virus is cleared, we observe a distinct transcriptional profile emerge (Fig. 1*F*). Over the course of the 24 d, we found three categories of gene regulation that were of interest: transient up-regulation during infection (Fig. 1*G*), up-regulation after clearance of viral RNA (Fig. 1*H*), or down-regulation during or after infection (Fig. 1*I*). To verify that this gene regulation also occurred in vivo, we next infected transgenic mice (13) with IAV-Cre to fluorescently label surviving cells (Fig. S2). On days 0, 5, 21, and 50 postinfection, we sorted CD45-negative, reporter-positive

Significance

After influenza A virus infection, the host is protected from subsequent unrelated respiratory virus infections for a temporary period. Although this phenomenon has been reported both in animal models and human clinical data, the mechanism for this antiviral immunity is incompletely understood. In this article, we demonstrate that club cells surviving direct infection by influenza A virus are reprogramed to promote an antiviral lung environment, and the depletion of "survivor cells" eliminates the postinfluenza window of nonspecific immunity. These findings demonstrate a type of immunity that does not fit into the classical innate or adaptive models and may inform the future designs of vaccines, where eliciting nonspecific immunity would be beneficial.

Author contributions: J.R.H., J.K.L., R.A.L., P.P., and N.S.H. designed research; J.R.H., R.A.L., and N.S.H. performed research; J.R.H., D.S., J.K.L., R.A.L., P.P., and N.S.H. analyzed data; and J.R.H., P.P., and N.S.H. wrote the paper.

The authors declare no conflict of interest.

This article is a PNAS Direct Submission.

Data deposition: The data reported in this paper have been deposited in the Gene Expression Omnibus (GEO) database, www.ncbi.nlm.nih.gov/geo (accession no. GSE77734).

[1]To whom correspondence should be addressed. Email: nicholas.heaton@duke.edu.

This article contains supporting information online at www.pnas.org/lookup/suppl/doi:10.1073/pnas.1522376113/-/DCSupplemental.

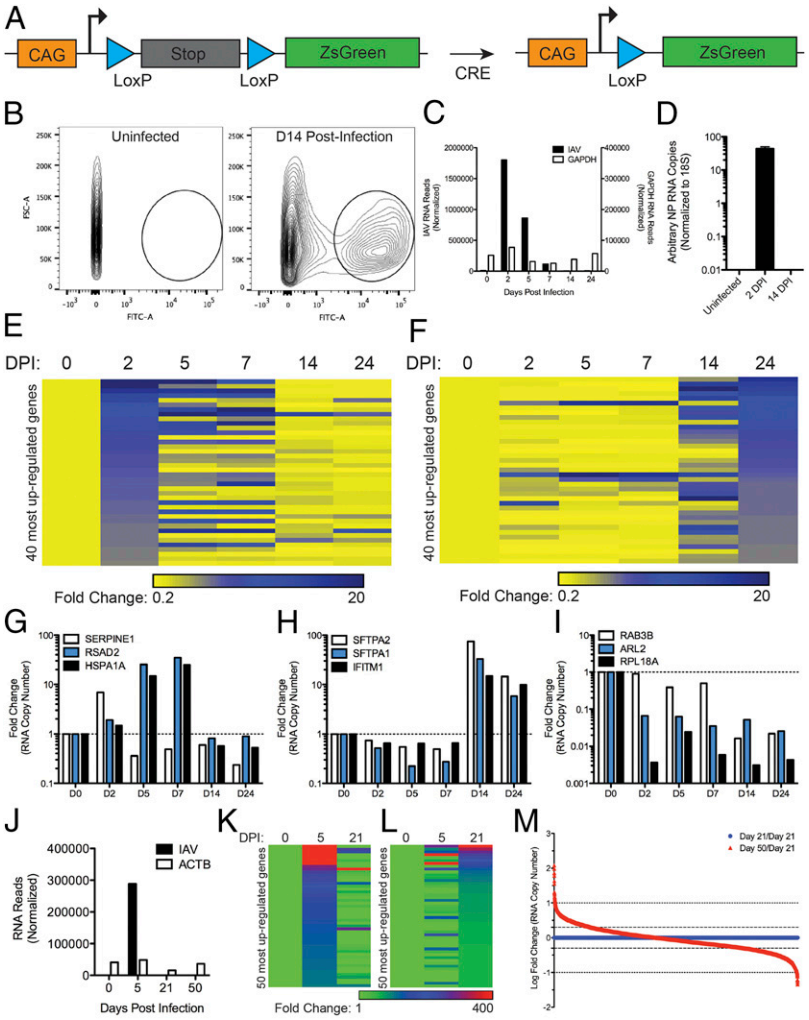

Fig. 1. Cells that survive IAV infection have stably altered profiles in vitro and in vivo. (*A*) Diagram of the Cre/LoxP system used to identify survivor cell populations via zsGreen protein production. (*B*) Flow cytometry plot of a human H441 cell line stably transduced with the Cre reporter construct before and 14 d after IAV-Cre infection. (*C–I*) Human H441 Cre reporter cells were infected with IAV-Cre over a period of time. At the indicated days, RNA was collected and analyzed from reporter-positive cells. (*C*) RNAseq quantification of viral or GAPDH mRNA from H441 Cre reporter cells at the indicated days postinfection. (*D*) IAV qRT-PCR assay for all forms of viral RNA in H441 Cre reporter cells at the indicated days postinfection. (*E*) RNAseq heat map of the top 40 RNA transcripts from Cre reporter-positive cells (as in *C*) at the indicated days postinfection ordered by the most up-regulated genes on day 2 postinfection. (*F*) Same data as in *E*, but ordered by the most up-regulated genes on day 24 postinfection. (*G–I*) Three major types of gene regulation after infection and survival: transient up-regulation (*G*), delayed up-regulation (*H*), and down-regulation (*I*). (*J–M*) Transgenic mice harboring a fluorescent Cre reporter cassette were infected with IAV-Cre, and reporter-positive cells were isolated at the indicated points. (*J*) RNAseq transcripts from viral or beta-actin (ACTB) mRNA from reporter-positive CD45$^-$ cells. (*K* and *L*) RNAseq of the top 50 RNA transcripts ordered by the most up-regulated genes at day 5 (*K*) or 21 (*L*) postinfection. (*M*) Changes in gene expression (of genes with ≥100 reads) in survivor cells isolated from mice at days 21 and 50 postinfection. Lines indicate two- and 10-fold changes.

cells [a population we have previously shown to be predominantly, but not necessarily exclusively, club cells (12)] and performed RNAseq. As expected, high levels of viral mRNA are detected after infection and are subsequently cleared (Fig. 1*J*). We again observed an antiviral response 5 d after infection (Fig. 1*K*) and a distinct transcriptional profile after viral clearance (Fig. 1*L*). Finally, we compared gene expression at 21 and 50 d postinfection to assess stability of the transcriptional changes (Fig. 1*M*). The expression level of most genes (99.4%) changed less than 10-fold.

To understand whether the altered state of survivor cells affected their response to subsequent stimuli, we subjected either naive or survivor H441 cells to WT IAV infection. Through several complementary assays, survivor H441 cells were found to be fully capable of supporting subsequent influenza virus infection. Naive and survivor cells were equally infected by IAV (Fig. S3 *A–C*), although we did observe a small but statistically significant reduction in the quantity of surface-expressed HA on surviving cells (Fig. S3*D*). When we assessed transcriptional profiles of cells responding to a primary or secondary infection, we found major differences (Fig. 2*A*). The differential response cannot be explained by unequal infection levels (Fig. 2*B* and Fig. S3) or maintained interferon-stimulated gene (ISG) expression from the primary infection (Fig. 2*C*). Interestingly, many but not all ISGs were up-regulated to a greater extent during the secondary infection (Fig. 2 *D* and *E*). We hypothesized this was a result of a potentiation of IFN signaling in surviving cells. We therefore treated naive or survivor H441 cells with IFN alpha and performed qRT-PCR for the ISGs: *IRF7* (Fig. 2*F*), *RIG-I* (Fig. 2*G*), and *ISG15* (Fig. 2*H*). As expected, viral secondary infection was not required to reproduce the increased IFN response in the surviving cell populations.

To verify that the differential response to secondary infection was recapitulated in vivo, we infected transgenic reporter animals that survived a primary infection with IAV-Cre with a heterologous mouse-adapted influenza B virus (IBV) strain (B/Malaysia/2056/04). There is no cross protection between IAV and IBV (14), allowing specific interrogation of innate immune processes. During the secondary infection, CD45-negative cells surviving the primary infection were sorted, and as with the in vitro data, a significantly different response to secondary infection was observed (Fig. 2*I*). Surviving cells cleared the primary infection and were actively infected during the secondary infection (Fig. 2*J*). To control for potential differences between the immune response to IAV and IBV, mice received a primary infection with each, and the responses of infected cells were compared (Fig. 2*K*). The response was similar, supporting our hypothesis that in vivo survivor cells respond differently to secondary infection. In addition, ISGs up-regulated during primary infection returned to baseline by the secondary infection (Fig. 2*L*), and many ISGs were transcribed at higher levels during the secondary infection (Fig. 2*M*). On the basis of these in vitro and in vivo data, we conclude that the transcriptional alteration of surviving cells has functional consequences during secondary viral infection and type I IFN signaling.

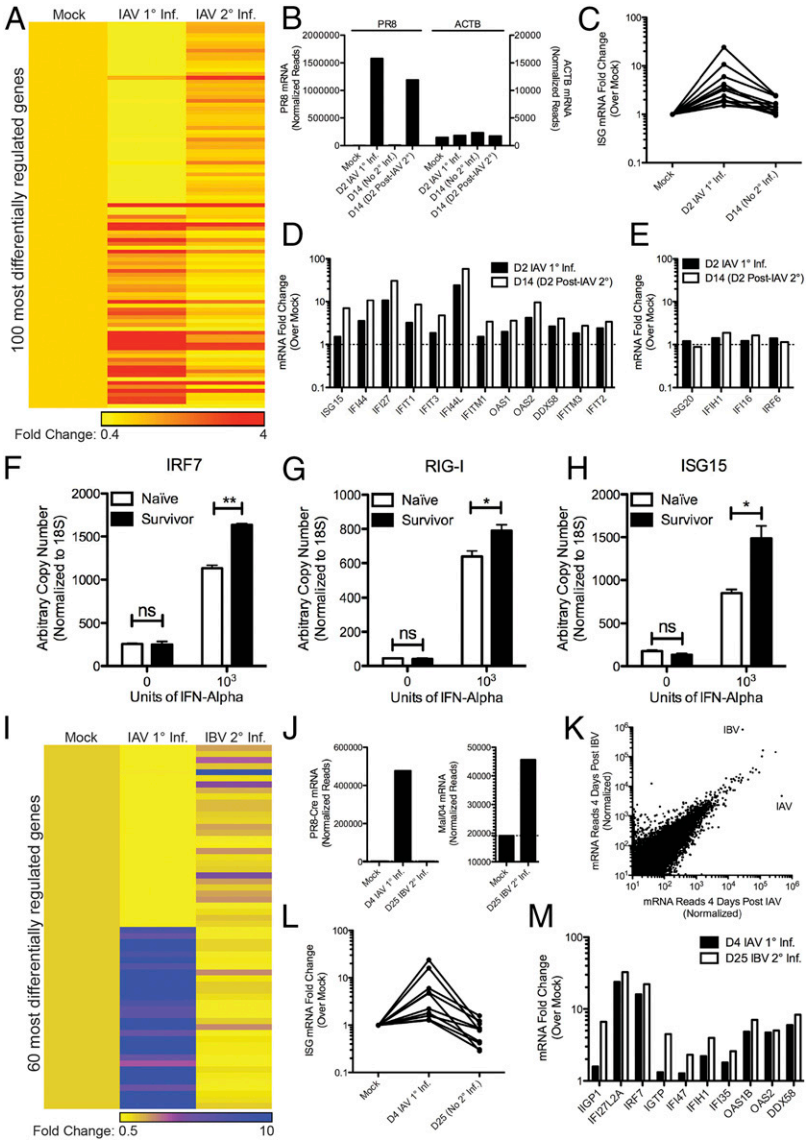

Fig. 2. Survivor cells respond differently to secondary infection and type I IFN stimulation in vitro and in vivo. (*A–D*) Human H441 cells were infected with WT-IAV at a multiplicity of infection (MOI) of 2.5; 12 d postprimary infection, cells were reinfected with WT-IAV at the same MOI, and cells were sequenced 2 d postsecondary infection. (*A*) RNAseq heat map representation of the top 100 RNA transcripts from H441 cells, as ordered by the most differentially regulated transcripts between the primary and secondary infection. (*B*) ACTB and viral RNA transcripts from *A*. (*C*) Representative expression levels of a subset of ISGs during primary infection (day 2) and after viral clearance (day 14). (*D* and *E*) Expression levels of a subset of ISGs during the primary and secondary infections (from *A*). (*F–H*) Stimulation of naive or survivor H441 cells with 1,000 U of IFN-alpha for 24 h and qRT-PCR of the ISGs: IRF7 (*F*), RIG-I (*G*), or ISG15 (*H*). Error bars represent SEM. (*I–M*) Transgenic Cre reporter mice were infected with IAV-Cre; 22 d postprimary infection, mice were infected with IBV and reporter-positive cells were isolated 3 d postsecondary infection. For the primary infection, reporter-positive cells were isolated at 4 d postinfection with IAV-Cre. (*I*) RNAseq heat map representation of the top 60 RNA transcripts from mouse reporter-positive CD45$^-$ cells, as ordered by the most differentially regulated transcripts between the primary (IAV) and secondary (IBV) infection. (*J*) IAV and IBV viral mRNA transcripts from *I*. The dotted lines indicate the background levels of detection. (*K*) Transcriptional response of primary infections in mouse CD45$^-$ lung cells to IBV (*y* axis) and IAV (*x* axis). Labeled data points indicate viral mRNA. (*L*) Representative expression of a subset of ISGs during primary infection (D4) and postviral clearance (D25). (*M*) Expression levels of a subset of ISGs during the primary and secondary infections (from *I*). For all panels: $*P \leq 0.05$; $**P \leq 0.001$; ns, not significant.

We reasoned that reprogrammed surviving cell populations could potentially contribute to the temporary window of antiviral immunity observed after influenza virus infection. To investigate this, we first tested the existence of a temporary window of nonspecific immunity after IAV infection. Mice received an infection with IAV, and at various intervals postinfection, the median lethal dose of IBV was determined (Fig. 3*A*). At the time of secondary infection, we verified that no infectious IAV remained (Fig. S4*A*) and that no IBV cross-reactive antibodies were generated from the primary infection (Fig. S4*B*). On IBV infection, we observed a striking difference in morbidity and mortality between naive mice and mice challenged 3 wk prior with IAV (Fig. 3 *B* and *C*). Interestingly, this protection waned by 6 wk postprimary infection and was almost completely undetectable by 12 wk (Fig. 3 *B* and *C*). This window of immunity is dependent on viral replication and cannot be explained by intranasal treatment with IFN alone (15). Temporary protection over this short period strongly argues against a classical adaptive immune response and fits with our model of a temporary window of enhanced innate immunity mediated by survivor cells. Presumably the turnover or alteration of survivor cells during lung remodeling/repair (16, 17) could be responsible for the temporal aspect of this protection.

We next assessed hematoxylin and eosin-stained lung sections from mice experiencing either a primary or secondary IBV infection (Fig. 3*D*). Although both groups exhibited epithelial damage, we observed a significant increase in inflammation during the secondary infection (Fig. 3 *E–H*). The localization of infiltration also differed: Most immune cells were peribronchiolar during the secondary infection, whereas intraluminal infiltration was observed during the primary infection.

Broad immunophenotyping of the immune cells (Fig. S5) in both the bronchoalveolar lavage (BAL) and the lung tissue was next performed. In agreement with the histology data, there were significantly fewer cells in the BAL of animals experiencing a secondary infection, despite there being more cells overall in the lung itself (Fig. 4*A*). Significantly fewer monocytes and neutrophils were found in the BAL during the secondary infection, but no change in dendritic cell/macrophage numbers (Fig. 4 *B–D*). Interestingly, the dendritic cell/macrophage population expressed higher levels of MHCII during the secondary infection (Fig. 4*E*). B cells and T cells showed the opposite trend of neutrophils and monocytes, with significantly more present in the BAL during the secondary infection (Fig. 4 *F* and *G*). When comparing the percentages of each cell population, we observed no major changes in the lung (Fig. 4*H*), but there were striking differences in immune cell composition of the BAL (Fig. 4*I*).

We next measured cytokines and chemokines to understand how infiltration was being altered during secondary infection. We observed that the vast majority of these molecules was detected in higher amounts during primary infection relative to secondary infection (Fig. 4*J*). Many factors were detected at much lower levels, including TNF-alpha, a major contributor to lung disease during influenza virus infection (18). In fact, only two factors (IL-12 and IFN-gamma) were expressed at a higher level in the BAL during secondary infection (Fig. 4*K*). As the CD45-negative surviving cells sit directly in the respiratory epithelial layer separating the lung from the BAL, these cells could be contributing to the control of chemokine/cytokine signaling and/or cellular infiltration.

To probe how surviving cells may be contributing to altered cytokines/chemokines in the BAL, we determined their transcriptional levels during primary and secondary IBV infections. Underscoring how survivors respond differently than naive cells, we observed a range of changes (Fig. 4*L*). Several genes (*TNF*, *IL6*, *GM-CSF*, *CXCL1*, *CXCL2*, *CCL20*) were transcribed in lower amounts during secondary infection. Survivors also expressed increased levels of two isoforms of the immunosuppressive cytokine *TGF-β* during secondary infection (Fig. 4*M*). Thus, survivor cells may both directly and indirectly contribute to the altered levels of cytokines and chemokines. Analysis of viral titers revealed a significant 10-fold reduction during the secondary infection, which suggests that the changes in cellular infiltration and cytokine profiles are better suited to controlling viral replication (Fig. 4*N*).

To test the surviving cells' contribution to nonspecific immunity, we used a transgenic mouse expressing the diphtheria toxin (DT) receptor after Cre-mediated recombination (19). Mice were infected with a sublethal dose of IAV-Cre and, after recovery, were administered either DT to specifically deplete surviving cells or PBS as a control. Lungs 21 d postinfection maintained high numbers of club cells after DT treatment, suggesting survivor cells represent a small proportion of the total club cell population in the lung (Fig. S6). When mice were subsequently challenged with IBV on day 21, we observed increased morbidity and mortality in the DT-treated mice (Fig. 4 *O* and *P*), demonstrating that survivor cells contribute to the temporary nonspecific viral immunity observed after IAV infection.

Discussion

We have provided evidence that cells survive direct viral infection, which causes long-term genetic changes. These changes alter the way the cells respond to secondary infection and type I IFN stimulation. Antigen-nonspecific immunity exists for a period of a few weeks after IAV infection and is correlated with changes in the composition of cellular infiltration and cytokine/chemokine profiles. Importantly, we demonstrated that survivor cells are required for this immunity: When survivor cells are depleted, mice are not protected from secondary infection.

Although numerous reports detail how tissues are remodeled after infection (16, 17, 20–22), and how residual (or tissue resident) immune cells influence immune responses (23–28), this report is, to our knowledge, the first to demonstrate that previously infected cells contribute to this environment. Although our in vitro studies have characterized the survival of club cells, additional cellular populations may survive IAV infection in vivo and may also be contributing to the observed protection phenotype.

Our results suggest that an active host immune program exists to prevent a secondary infection from a previously unencountered viral pathogen. In contrast to classical adaptive immunity, which is

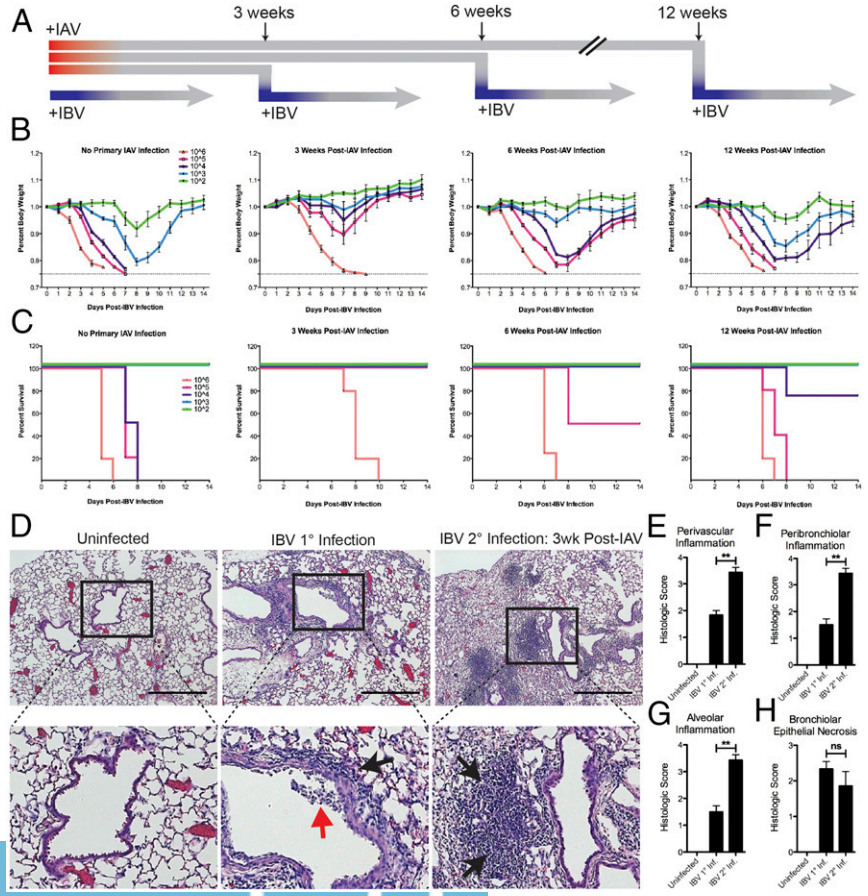

Fig. 3. Temporary, antigen-nonspecific immunity is induced after IAV infection. (*A*) Summary of the primary and secondary infection schedule of C57BL/6 mice. (*B*) Percentage initial body weight of animals infected with IBV without IAV primary infection (*Left*) or 3, 6, or 12 wk after primary infection with IAV (*Right*). Dashed line indicates the humane endpoint of 75% of starting body weight; error bars represent SEM. (*C*) Animal survival from data shown in *B*. (*D*) Hematoxylin and eosin-stained lung sections from uninfected animals, IBV-infected animals with no primary infection, and IBV-infected animals 3 wk after IAV primary infection. Animals were infected with 10^5 plaque forming units (PFU) of IBV, and lungs were collected 3 days postinfection. (Scale bar, 400 μm.) Insets are indicated by the boxed regions. Black arrowheads indicate peribronchiolar inflammation, and red arrowheads indicate intraluminal infiltration and debris. (*E–H*) Independent pathology quantification of inflammation and epithelial necrosis as indicated. Error bars indicate the SEM. For all panels: $*P \leq 0.05$; $**P \leq 0.001$.

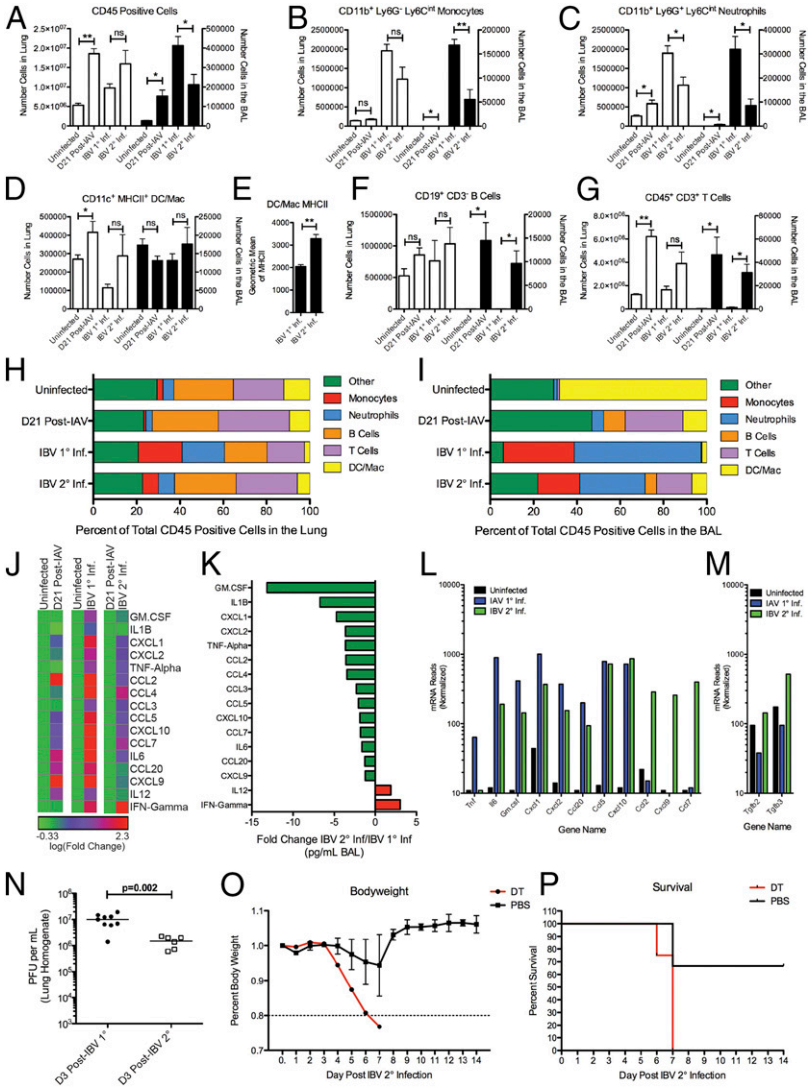

Fig. 4. Survivor cells contribute to the antiviral lung environment that is established after IAV infection. (*A–G*) C57BL/6 mice were infected with a sublethal dose (50 PFU) of WT IAV. Twenty-one days postinfection, mice were challenged with a secondary infection of 10^5 PFU of IBV. Three days postsecondary infection, BAL fluid and lung tissue were collected for immune cell phenotyping by flow cytometry. Total numbers of lung (white bars) and BAL (black bars): $CD45^+$ cells (*A*), $CD45^+CD11b^+Ly6G^-Ly6C^{int}$ monocytes (*B*), $CD45^+CD11b^+Ly6G^+Ly6C^{int}$ neutrophils (*C*), $CD45^+CD11c^+MHCII^+$ dendritic cells/macrophages (*D*), MHCII surface expression on dendritic cells/macrophages (*E*), $CD45^+CD19^+CD3^-$ B cells (*F*), and $CD45^+CD3^+$ T cells (*G*). (*H* and *I*) Percentages of total $CD45^+$ cells in the lung (*H*) and BAL (*I*). (*J*) Heat map representation of $\log_{10}$ fold changes of cytokine/chemokine protein levels in BAL from the indicated treatments. (*K*) Fold change in cytokine/chemokine protein levels in BAL comparing IBV secondary infection with IBV primary infection. (*L* and *M*) Cytokine/chemokine RNA transcript levels in survivor cells during primary and secondary IBV infections. (*N*) IBV lung titers in primary and secondary infected animals. (*O*) Diphtheria toxin receptor Cre reporter animals were given a sublethal primary infection with IAV-Cre. Sixteen and 17 d postinfection, survivor cell populations were depleted via DT administration. Twenty-one days postprimary infection, animals were challenged with 5.6×10^5 PFU IBV, and body weight (*O*) and survival (*P*) were monitored. Error bars represent SEM. For all panels: $*P \leq 0.05$l $**P \leq 0.001$; ns, not significant.

highly antigen-specific, reprogrammed survivor cells provide a window of protection after clearance of the first virus. This protection was not simply a prolonged window of antiviral signaling by the survivor cells, but a distinct response (and/or an increased response) to the secondary infection. It is tempting to speculate that this temporary nonspecific antiviral immunity may have evolved to protect the host during the lung repair period after the primary infection. Understanding how to induce survivor-like cell populations may potentially inform the development of broadly antiviral therapeutics, as well as more clinically effective live-attenuated vaccines.

Future studies are required to understand how survivor cells drive nonspecific immunity. The protective effects are likely indirect, modulating either the recruitment or retention of professional immune cells. Although our data show that both cytokines and cellular infiltration are modulated when surviving cells are present, the distinct correlates of protection remain unclear. In conclusion, we have provided evidence that the cells that survive direct IAV infection have profound effects on the immune status of the host. Therefore, we propose that cells surviving infection (and their subsequent effect on pathogenesis and immunity) represent an additional mechanism of protection against viral pathogens.

Materials and Methods

Tissue Culture. H441, 293T, and MDCK cells were used in this study (ATCC). H441 cells (a human club cell-like line) were maintained in RPMI-1640 (ATCC), MDCK cells were maintained in EMEM (Gibco), and 293T cells were maintained in DMEM (Gibco). All media was supplemented with 10% (vol/vol) FCS, L-glutamine, and Pen/Strep. Development of the H441-CR cells is described in the *SI Materials and Methods*.

Animal Experiments. WT, female C57BL/6 mice were purchased (Jackson) at 8–10 wk old. C57BL/6-*Gt(ROSA)26Sor*$^{tm1(HBEGG)Awai}$/J) and B6.Cg-*Gt(ROSA)26Sor*$^{tm14(CAG-tdTomato)Hze}$/J were also purchased (Jackson) and bred on site. Animal infections are detailed in the *SI Materials and Methods*. All experiments involving animals were performed in accordance with the Icahn School of Medicine at Mount Sinai Animal Care and Use Committee.

Flow Cytometry. Flow cytometry analysis of H441-CR cells was performed by scraping cells into FACS buffer (PBS containing 1% BSA). After pelleting at 240 × *g*, cells were resuspended in PBS and stained with LIVE/DEAD Fixable Blue Dye (Life Technologies) for 10 min on ice. Live cells were assessed for zsGreen expression. BAL was performed to isolate infiltrating immune cells from murine lungs: 1 mL PBS was injected through the trachea to inflate lungs and subsequently aspirated for collection. BAL fluid was centrifuged at 240 × *g*, supernatant was frozen at −80 °C for Luminex analysis. Cells from the BAL or lungs were collected and processed for flow cytometry analysis, as described in the *SI Materials and Methods*.

FACS. Cells were isolated using a FACS Aria cell sorter (BD) and sorted directly into lysis buffer containing RNase inhibitor (Takara Bio Inc.). To isolate reporter-positive H441-CR cells, culture flasks were scraped to collect cells, which were then passed through a 70-μm filter (Falcon) and resuspended in FACS buffer, and then zsGreen-positive cells were sorted. For assessing cells infected and/or surviving infection in vivo, lungs were perfused with PBS and treated with dispase (Corning), as described earlier. For sorting out cells from mice experiencing a primary infection from IAV-Cre or B/Malaysia/2506/04, polyclonal serum from mice infected with these viruses was used at a 1:1,000 dilution, followed by staining with Alexa Fluor 488 anti-mouse secondary (Thermo Fisher Scientific) at a 1:1,000 dilution. For sorting out surviving cells during secondary influenza virus challenge, tdTomato-positive cells (indicating IAV-Cre survivors) were sorted. In both primary and secondary influenza virus challenge experiments, anti-CD45 antibody (30-F11; BD) was used to specifically isolate CD45-negative cells.

qRT-PCR. RNA was isolated either through TRIzol extraction (Life Technologies) or the 96 RNeasy kit (QIAGEN). SuperScript III Platinum One-Step qRT-PCR kit (Life Technologies) was used for reverse-transcription and TaqMan FAM-labeled probes were used for IRF7, RIG-I, and ISG15 quantification of gene expression (Life Technologies). A custom IAV TaqMan assay is described in *SI Materials and Methods*. Copy number values were normalized to a VIC-labeled eukaryotic 18S ribosomal RNA probe (Thermo Fisher), and arbitrary copy numbers were assigned on the basis of a standard curve.

Luminex Cytokine and Chemokine Analysis. To assess cytokine and chemokines in lung BALs, mice were killed by cervical dislocation, and 1 mL PBS was used to isolate cells infiltrating the lungs. BALs were then pelleted for 10 min at 240 × *g*, and supernatant was transferred to a new tube and frozen at −80 °C. Cytokines and chemokines were assessed through a multiplex bead array assay, as previously described (12).

Next-Generation mRNA Sequencing. RNA was sequenced as previously described (12) and detailed in *SI Materials and Methods*. Resulting reads were mapped to the mouse or human transcriptome, as well as the influenza virus genome, via Bowtie. Samples were run either on Basespace (Illumina) or Mount Sinai's high-performance computing cluster. In determining the fold changes between conditions, total read numbers were normalized, and all values were increased by 10 reads to minimize the outlier effects of extremely small read numbers. Heat maps were generated via methods described elsewhere (29). Raw sequencing data and mapped reads are available in the Gene Expression Omnibus database under series accession number GSE77734.

Statistical Analysis. Unless specifically noted, all statistical analysis between datasets was performed using a two-tailed Student's *t* test in Prism software (GraphPad). Differences were considered significant when $P \leq 0.05$.

ACKNOWLEDGMENTS. We acknowledge Virginia Gillespie for her expertise in scoring the lung sections, Carlos Rodriguez for assistance with the multiplexed cytokine analysis, Rebekah Dumm for assistance with microscopy, and Matthew Evans and Marion Sourisseau for their expertise and help with the generation of the retrotransduced H441 cell line. We also acknowledge the use of the Mount Sinai Microscopy Shared Resource Facility, the Genomics Core Facility, the Biorepository and Pathology Center of Research Excellence (CORE), and the Flow Cytometry Shared Resource Facility. This work was partially supported by HHSN272201400008C (P.P.), U19 AI109946 (P.P.), F31AI120648 (J.R.H.), and K22AI116509 (N.S.H.).

1. Walzl G, Tafuro S, Moss P, Openshaw PJ, Hussell T (2000) Influenza virus lung infection protects from respiratory syncytial virus-induced immunopathology. *J Exp Med* 192(9):1317–1326.
2. Laurie KL, et al. (2010) Multiple infections with seasonal influenza A virus induce cross-protective immunity against A(H1N1) pandemic influenza virus in a ferret model. *J Infect Dis* 202(7):1011–1020.
3. Laurie KL, et al. (2015) Interval Between Infections and Viral Hierarchy Are Determinants of Viral Interference Following Influenza Virus Infection in a Ferret Model. *J Infect Dis* 212(11):1701–1710.
4. Cowling BJ, et al. (2012) Increased risk of noninfluenza respiratory virus infections associated with receipt of inactivated influenza vaccine. *Clin Infect Dis* 54(12): 1778–1783.
5. Piedra PA, et al. (2005) Live attenuated influenza vaccine, trivalent, is safe in healthy children 18 months to 4 years, 5 to 9 years, and 10 to 18 years of age in a community-based, nonrandomized, open-label trial. *Pediatrics* 116(3):e397–e407.
6. Kelly H, Barry S, Laurie K, Mercer G (2010) Seasonal influenza vaccination and the risk of infection with pandemic influenza: A possible illustration of non-specific temporary immunity following infection. *Euro Surveill* 15(47):19722.
7. Cowling BJ, Nishiura H (2012) Virus interference and estimates of influenza vaccine effectiveness from test-negative studies. *Epidemiology* 23(6):930–931.
8. Ferguson NM, Galvani AP, Bush RM (2003) Ecological and immunological determinants of influenza evolution. *Nature* 422(6930):428–433.
9. Hirsh S, et al. (2014) Epidemiological changes of respiratory syncytial virus (RSV) infections in Israel. *PLoS One* 9(3):e90515.
10. Casalegno JS, et al. (2010) Impact of the 2009 influenza A(H1N1) pandemic wave on the pattern of hibernal respiratory virus epidemics, France, 2009. *Euro Surveill* 15(6):19485.
11. Mak GC, Wong AH, Ho WY, Lim W (2012) The impact of pandemic influenza A (H1N1) 2009 on the circulation of respiratory viruses 2009-2011. *Influenza Other Respi Viruses* 6(3):e6–e10.
12. Heaton NS, et al. (2014) Long-term survival of influenza virus infected club cells drives immunopathology. *J Exp Med* 211(9):1707–1714.
13. Madisen L, et al. (2010) A robust and high-throughput Cre reporting and characterization system for the whole mouse brain. *Nat Neurosci* 13(1):133–140.
14. Krammer F, Pica N, Hai R, Margine I, Palese P (2013) Chimeric hemagglutinin influenza virus vaccine constructs elicit broadly protective stalk-specific antibodies. *J Virol* 87(12):6542–6550.
15. Bracci L, et al. (2005) Type I IFN is a powerful mucosal adjuvant for a selective intranasal vaccination against influenza virus in mice and affects antigen capture at mucosal level. *Vaccine* 23(23):2994–3004.
16. Yahaya B (2012) Understanding cellular mechanisms underlying airway epithelial repair: Selecting the most appropriate animal models. *ScientificWorldJournal* 2012: 961684.
17. Crosby LM, Waters CM (2010) Epithelial repair mechanisms in the lung. *Am J Physiol Lung Cell Mol Physiol* 298(6):L715–L731.
18. La Gruta NL, Kedzierska K, Stambas J, Doherty PC (2007) A question of self-preservation: Immunopathology in influenza virus infection. *Immunol Cell Biol* 85(2):85–92.
19. Buch T, et al. (2005) A Cre-inducible diphtheria toxin receptor mediates cell lineage ablation after toxin administration. *Nat Methods* 2(6):419–426.
20. Monticelli LA, et al. (2011) Innate lymphoid cells promote lung-tissue homeostasis after infection with influenza virus. *Nat Immunol* 12(11):1045–1054.
21. Holtzman MJ, Byers DE, Alexander-Brett J, Wang X (2014) The role of airway epithelial cells and innate immune cells in chronic respiratory disease. *Nat Rev Immunol* 14(10):686–698.
22. Hogan BL, et al. (2014) Repair and regeneration of the respiratory system: Complexity, plasticity, and mechanisms of lung stem cell function. *Cell Stem Cell* 15(2): 123–138.
23. Moyron-Quiroz JE, et al. (2004) Role of inducible bronchus associated lymphoid tissue (iBALT) in respiratory immunity. *Nat Med* 10(9):927–934.
24. Wakim LM, Gupta N, Mintern JD, Villadangos JA (2013) Enhanced survival of lung tissue-resident memory CD8$^+$ T cells during infection with influenza virus due to selective expression of IFITM3. *Nat Immunol* 14(3):238–245.
25. Sheridan BS, Lefrançois L (2011) Regional and mucosal memory T cells. *Nat Immunol* 12(6):485–491.
26. Quintin J, Cheng SC, van der Meer JW, Netea MG (2014) Innate immune memory: Towards a better understanding of host defense mechanisms. *Curr Opin Immunol* 29: 1–7.
27. Schenkel JM, et al. (2014) T cell memory. Resident memory CD8 T cells trigger protective innate and adaptive immune responses. *Science* 346(6205):98–101.
28. Schenkel JM, Masopust D (2014) Tissue-resident memory T cells. *Immunity* 41(6): 886–897.
29. Pavlidis P, Noble WS (2003) Matrix2png: A utility for visualizing matrix data. *Bioinformatics* 19(2):295–296.
30. Hermann M, et al. (2014) Binary recombinase systems for high-resolution conditional mutagenesis. *Nucleic Acids Res* 42(6):3894–3907.
31. Sourisseau M, et al. (2013) Temporal analysis of hepatitis C virus cell entry with occludin directed blocking antibodies. *PLoS Pathog* 9(3):e1003244.